ChemPubSoc Europe

DOI: 10.1002/open.201402133

Open Access ChemistryOPEN Full Papers

Preparation and Characterization of Chitosan Thin Films on Mixed-Matrix Membranes for Complete Removal of Chromium

Vignesh Nayak,[a] Mannekote Shivanna Jyothi,[a] R. Geetha Balakrishna,*[a] Mahesh Padaki,*[a] and Ahmad Fauzi Ismail[b]

Herein we present a new approach for the complete removal of Cr^{VI} species, through reduction of Cr^{VI} to Cr^{III}, followed by adsorption of Cr^{III}. Reduction of chromium from water is an important challenge, as Cr^{IV} is one of the most toxic substances emitted from industrial processes. Chitosan (CS) thin films were developed on plain polysulfone (PSf) and PSf/TiO_2 membrane substrates by a temperature-induced technique using polyvinyl alcohol as a binder. Structure property elucidation was carried out by X-ray diffraction, microscopy, spectroscopy, contact angle measurement, and water uptake studies. The increase in hydrophilicity followed the order: PSf < PSf/TiO_2 < PSf/TiO_2/CS membranes. Use of this thin-film composite membrane for chromium removal was investigated with regards to the effects of light and pH. The observations reveal 100% reduction of Cr^{VI} to Cr^{III} through electrons and protons donated from OH and NH_2 groups of the CS layer; the reduced Cr^{III} species are adsorbed onto the CS layer via complexation to give chromium-free water.

Introduction

Water is the source of life for plants, animals, and the human population. Stress on water resources is increasing daily due to various human activities, leading to increased environmental damage. Contamination of water by the presence of heavy metals such as chromium is of serious concern.[1] The discharge of chromium from activities such as leather tanning, pigment production, steel fabrication, and mining[2] needs to be addressed. Chromium is mainly present in two stable oxidation states, Cr^{III} and Cr^{VI}, the latter of which is considered to be highly toxic and carcinogenic. Techniques currently available for the removal of chromium such as reduction,[3] precipitation,[4] ion exchange,[5] solvent extraction,[6] electroplating,[7] membrane separation,[8] and adsorption[9] each have their own advantages and disadvantages, including time consumption and recyclability; in this context the study presented herein was undertaken to prepare membranes for chromium elimination with superior qualities such as high efficiency, recyclability, and ease of processing. Among the various techniques available, membrane technology has received much recent attention in the separation process, because of its facile operation and high energy savings.[10] Polymers are considered to be among the important materials in membrane technology, given their good flexibility, toughness, and separation capacity.[11] Nano-filtration membranes play a prominent role in the removal of toxic heavy metals,[12] and more so the thin-film composite (TFC) membranes, which are an important class of nano-filtration membranes.[13] The TFC membranes, often used in separation processes, have a dense, thin, and selective skin layer and a micro-porous support layer prepared from various polymeric materials,[10] namely polysulfone (PSf), polyether sulfone, polyurethane, polyacrylonitrile, and polyvinyl difluoride.[14]

Chitosan (CS) has recently shown its impact in membrane separation. CS is a nontoxic, odorless, antibacterial, biocompatible, and biodegradable hetero-polysaccharide obtained by the N-deacetylation of a natural polymer chitin,[15,16] and serves as a very good material for membrane preparation. Chitin is found in the shells of crabs and prawns, and it is environmentally benign. CS is highly hydrophilic and has a sorption capacity for metal ions due to the presence of reactive amino and hydroxy groups; it is also soluble in organic acids through the protonation of NH_2 groups to NH_3^+. However, CS has low mechanical stability, and therefore its use in large scale is limited.[17] This problem can be overcome by chemically modifying CS or by applying CS as an active layer in TFC membranes for good mechanical strength. These composite membranes possess the combined properties of organic and inorganic materials such as high permeability, selectivity, and thermal and chemical resistance.[18] PSf is widely used as an organic support for composite membranes, as it has good chemical and thermal stability with high hydrophobicity.[10] The limitation of hy-

[a] V. Nayak, M. S. Jyothi, Prof. R. G. Balakrishna, Dr. M. Padaki
Center for Nano and Material Sciences
Jain University, Ramanagaram, Bangalore 562112 (India)
E-mail: geethabalakrishna@yahoo.co.in
maheshpadaki@gmail.com

[b] Prof. A. F. Ismail
Advanced Membrane Research Centre (AMTEC)
Universiti Teknologi Malaysia, UTM Skudai, 81310 Johor (Malaysia)

drophobicity is overcome by incorporating inorganic fillers within the organic polymer matrix. Nano-TiO_2 is one such inorganic filler that is stable, hydrophilic, and photoactive to facilitate reduction.[19] This can be an optimal constituent for imparting a hydrophilic nature to the PSf membrane.[20] In this regard, a CS thin film was developed on a PSf/TiO_2 composite membrane.

In this work, CS thin films were developed on PSf/TiO_2 composite membranes and were characterized by infrared spectroscopy, X-ray diffraction (XRD), scanning electron microscopy (SEM), contact angle measurement, and water uptake studies; they were compared with CS thin films developed on PSf membranes. The prepared membranes were used for the reduction of toxic Cr^{VI} to Cr^{III}. To the best of our knowledge, there are only few published reports of such attempts to reduce Cr^{VI} to Cr^{III}. Modrzejewska and Kaminski[21] reported Cr^{VI} removal by CS membranes used for chromium filtration under pressure; in a similar fashion, Samadi et al.[22] prepared Cu–TiO_2/CS nanocomposite thin films with polycarbonate as a support for the photocatalytic reduction of Cr^{VI} and Pb adsorption. PSf and PSf/TiO_2 membranes have only rarely been used as substrates for CS thin films. The novelty in this work is in the improved and facile method for the preparation of CS thin films and new substrates. Several experiments were conducted to determine the requirements for the feasibility of the reduction reactions; the adsorption of reduced Cr^{III} was also studied. The effect of pH and the influence of light exposure in causing reduction via photocatalytic titania was studied with respect to the removal of chromium. Moreover, the kinetics of the reduction were studied and are discussed herein with scientific rationale.

Results and Discussion

Coating CS as an active layer on PSf gives the required mechanical strength to CS. To bind PSf and CS together firmly, polyvinyl alcohol (PVA) was used as the binder. PVA has high chemical stability, mechanical strength, and is highly hydrophilic. The presence of numerous hydroxy groups facilitates the formation of hydrogen bonds with the amine and hydroxy groups of CS.[23,24] PVA also has high adhesive properties, which enhance its use as a binder.[25] Hydrophilic interactions provide better binding between the substrate and the thin-film active layer. TiO_2 nanoparticles (NPs) were immersed in PSf to prepare a hydrophilic substrate and to act as a photocatalyst.

Characterization

ATR-IR

The chemical composition was confirmed by ATR-IR spectroscopy. The spectra showed characteristic CS peaks at 1013 cm^{-1} (C–N stretch), 1584 cm^{-1} (N–H bending), and 3400–3800 cm^{-1} (O–H stretching). Bands at 1150 cm^{-1} (–SO_2 stretch), 1242 cm^{-1} (C–O–C linkage), and 2967 cm^{-1} (aliphatic C–H stretch) denote the presence of PSf. The two traces in Figure 1 show similar

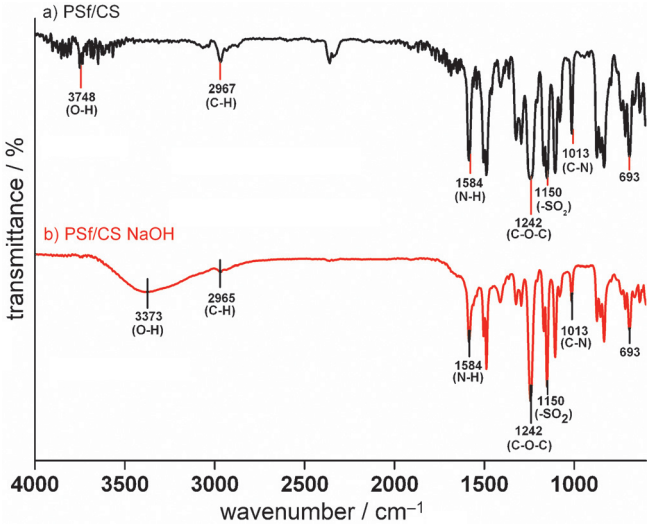

Figure 1. ATR-IR spectra of PSf/CS membranes a) before and b) after washing with NaOH solution.

spectral banding patterns except for the O–H stretching region. Figure 1 a depicts sharp O–H peaks due to intramolecular hydrogen bonding between the OH and NH_2 groups of CS, whereas Figure 1 b shows a broad peak for O–H stretching due to intermolecular hydrogen bonding.[26] Washing the membrane with a sodium hydroxide solution removes the trapped acetic acid, causing intermolecular hydrogen bonding between the active hydroxy and amino groups of CS and the hydroxy groups of PVA (Figure 2), leading to the stability of the membranes. Therefore, membranes washed with NaOH are more stable than unwashed membranes.

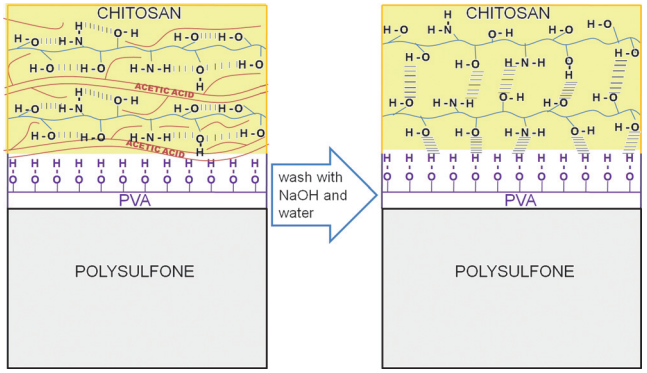

Figure 2. Representation of the formation of intermolecular hydrogen bonding networks between CS chains after treatment with NaOH and water.

XRD analysis

The X-ray diffraction patterns indicated the crystallinity and the nature of the interactions between the components in the prepared membranes. The simple mixed patterns of different components are expressed,[15] as there was no chemical interaction between the components of the membrane. The various components in the prepared membranes showed their

own crystal region. The TiO_2 NPs revealed a 100% peak at $2\theta = 25.29^\circ$ with a d-spacing of 3.518 Å, signifying an anatase phase and a complete absence of rutile TiO_2.[27] The average crystal diameter of NPs calculated using Scherrer's equation is 29 nm as shown in Table 1. The surface area of the bare TiO_2 was found to be 88.47 $m^2 gm^{-1}$, with a pore volume of 0.02146 $cm^3 gm^{-1}$, which was sufficient to exhibit good photocatalytic activity.

Table 1. Crystallite size, d-spacing, and strain (ε) values for bare TiO_2 NPs and TiO_2 in membrane matrix.

	2θ [°]	d-spacing [Å]	Size [nm]	ε
TiO_2 NPs	25.29	3.518	29	5.3×10^{-3}
PSf/TiO_2	25.52	3.486	122	1.27×10^{-3}
PSf/TiO_2/CS	26.3	3.43	201	0.747×10^{-3}

XRD patterns of the PSf/TiO_2 hybrid membrane (Figure 3) authenticate the incorporation of TiO_2 NPs into the PSf polymer matrix with no significant difference in the 2θ value. In the

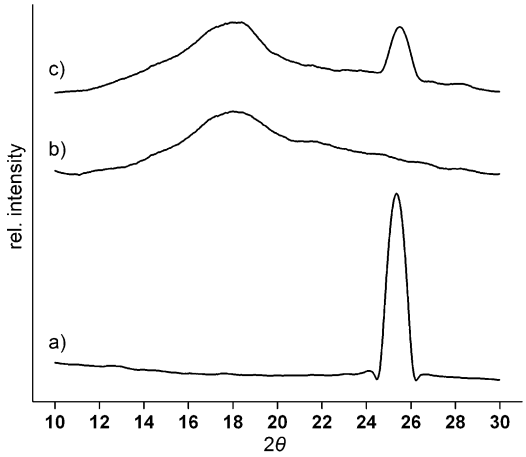

Figure 3. XRD patterns of a) TiO_2 NPs, b) plain PSf, and c) PSf/TiO_2.

case of PSf/TiO_2/CS (Figure 4), there is an immense shift of the TiO_2 peak to a higher 2θ value (Table 1). The microstrain appears high in TiO_2 NPs and is in agreement with Equation (1), which states that ε is inversely proportional to θ:

$$\varepsilon = \frac{\beta_{hkl}}{4\tan\theta} \quad (1)$$

β is the full-width half-maximum of the diffraction peak, and θ is Bragg's angle.[28]

The repulsive interaction between hydrophilic TiO_2 and hydrophobic PSf leads to the formation of free volume in the interstitial spaces between the polymer chains,[29] and this may cause a decrease in crystal strain, leading to the crystal growth of TiO_2 NPs. TiO_2 NPs also tend to self-assemble to form agglomerates. Hence the crystallite size increases drastically from

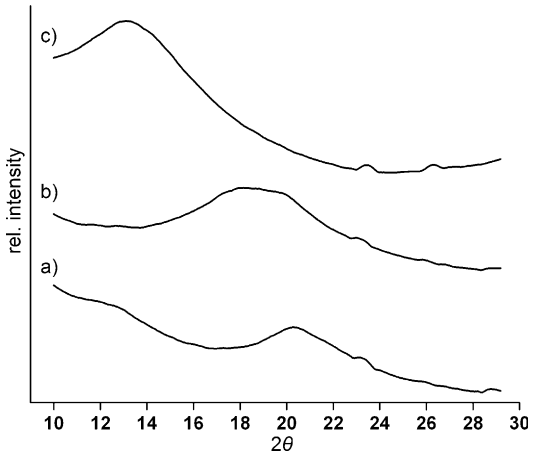

Figure 4. XRD patterns of a) plain CS, b) PSf/CS, and c) PSf/TiO_2/CS.

29 nm to 122 nm and to 201 nm for TiO_2 NPs, PSf/TiO_2, and PSf/TiO_2/CS, respectively.

In addition, the lattice parameters and crystal structure were altered, suggesting the deformation of the TiO_2 crystal structure due to interaction with the polymer chains. The height of the peaks (intensity) depends on the number of crystallites diffracting the X-rays, or the amount of phase exhibiting the reflection, and hence the greatest peak height is observed for TiO_2 NPs, and less intense peaks are observed for TiO_2 NPs distributed within the membranes.

SEM analysis

Scanning electron micrographs of the CS supported on plain PSf and PSf/TiO_2 membranes are presented in Figure 5. Figure 5a,b shows cross-sections of the PSf and PSf/TiO_2 membranes prepared by the phase-inversion technique. The cross-section of the PSf membrane (Figure 5a) is distinguished by three different layers: the top layer has small dense pores; this is followed by the intermediate layer, which shows medium pores with finger-like projections, and finally a thick sub-layer.

The PSf/TiO_2 support (Figure 5b,c) shows the same three layers, but their morphology is different from that of the PSf membrane. Figure 5b shows more finger-like projections than Figure 5a, and this is caused by hydrophilic TiO_2, where water as absorbed in the phase-inversion process. This also results in large pores, as observed below the finger-like projections of the membrane; this is in line with observations made by Emadzadeh et al.[30] The SEM images show that a thin layer of CS is properly cast on the top of the PSf support (Figure 5d). The thickness of the CS layer was determined by SEM analysis to be ~10–12 μm. As we spread the CS solution onto the support membrane, it did not penetrate into the finger-like projections, but instead settled onto the surface, thereby forming two separate layers, which is evident from the SEM images. The surface images give an overall view of the surface morphology of the membranes. From (Figure 5e) it can be observed that there is non-uniform distribution of the pores and TiO_2 NPs on the membrane surface, as has been the observa-

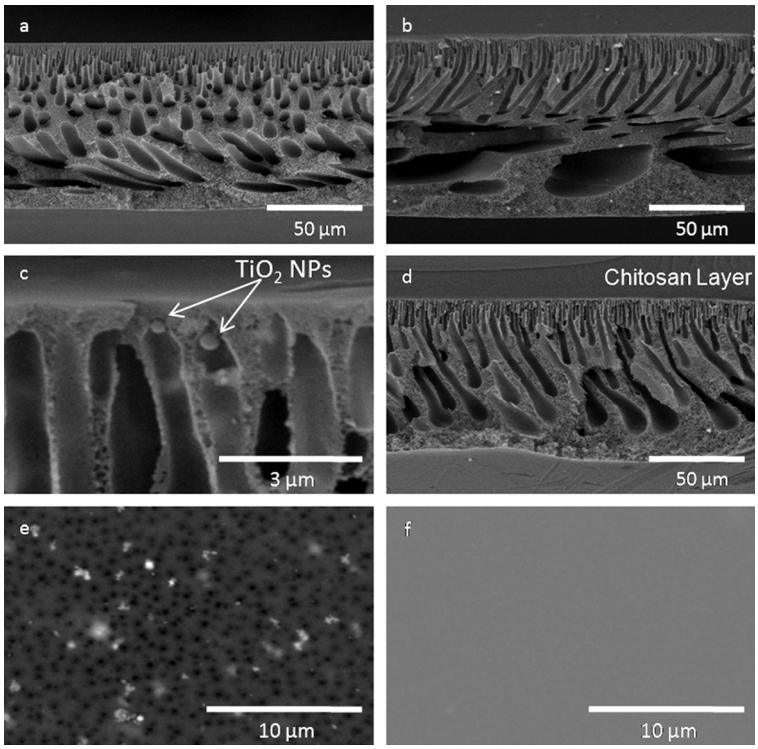

Figure 5. SEM images: cross-sections of a) PSf membrane, b), c) PSf/TiO_2 membrane, and d) PSf/CS membrane; surface images of e) PSf/TiO_2 membrane and f) PSf/TiO_2/CS membrane.

tion with many nanocomposites such as TiO_2[31] and silica[32] prepared by the phase-inversion process. As a thin layer of CS is coated on the surface of the PSf/TiO_2 support, all the pores were occupied by the CS solution, and a smooth-surfaced membrane was obtained (Figure 5 f) with pores in the nanometer size range.

Contact angle measurement

The hydrophilic nature of the prepared membranes was studied by measuring the contact angle for each membrane. Universally, the contact angle continues to decrease as the hydrophilic nature of the membranes increases.[33] The data in Figure 6 confirm that the hydrophilicity increases upon incorporation of TiO_2 NPs, and the contact angle decreases from 76° to 69°, mainly because TiO_2 has high affinity for water.[34] The contact angle of the PSf/TiO_2/CS membrane further decreases to 64°, as CS on the PSf/TiO_2 surface is highly hydrophilic due to the presence of hydrophilic OH and NH_2 groups; this is in agreement with results observed for PSf/CS blend membranes[35] and pHEMA and HEMA/CS membranes.[36]

Water uptake study

To study water uptake, prepared PSf/TiO_2/CS and PSf/CS membranes were dipped into water for 24 h at pH 4, 7, and 9. Figure 7 clearly indicates CS to have the highest affinity for water, with the PSf showing the lowest. Furthermore, the water uptake capacity decreases with increased pH. The CS membrane shows a higher absorption of water at acidic pH due to protonation of the amino groups present in the backbone of CS; this leads to chain relaxation, resulting in efficient solvent diffusion, and this phenomenon is not observed at basic or neutral pH. Incorporation of TiO_2 NPs further increases the hydrophilicity of the membrane. This is evident in Figure 7, in that PSf/TiO_2 and PSf/TiO_2/CS membranes have a greater capacity for water absorption than PSf and PSf/CS membranes, respectively. This results from the addition of TiO_2 NPs to the PSf polymer solution; owing to the high affinity of TiO_2 for water, it attracts more water during the diffusion process, and hence more water penetrates, creating larger and more numerous pores in the PSf membrane. The membrane can now absorb more water due to the increased number of pores, thus increasing its water uptake capacity.

Chromium reduction and adsorption studies

A series of experiments were carried out with PSf/TiO_2/CS and PSf/CS membranes in sunlight and dark. The reactions were performed at various pH levels and thus optimized. The results show complete Cr^{VI} reduction within 40 min, and no reduction at neutral

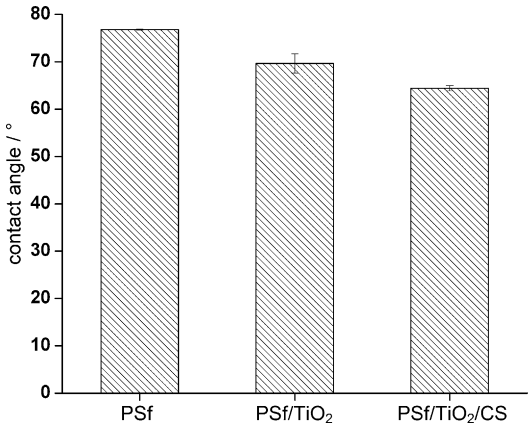

Figure 6. Contact angles of the membranes indicated; error bars represent the SD.

or basic pH. Because the results were not significant, they are not included here. The reduction process for Cr^{VI} to Cr^{III} can follow different mechanisms such as: 1) direct reduction of Cr^{VI} to Cr^{III} due to the presence of electron-donor groups present on the surface and then adsorption of Cr^{III} onto the binding sites through complexation, or 2) initial adsorption of Cr^{VI} species (mainly $HCrO_4^-$ and $Cr_2O_7^{2-}$) onto the surface and subsequent reduction of Cr^{VI} to Cr^{III} by the electron-donor groups.[37]

In the present work, route 1) is followed for Cr^{VI} reduction to Cr^{III}. Cr^{VI} is present in different forms depending on pH. At

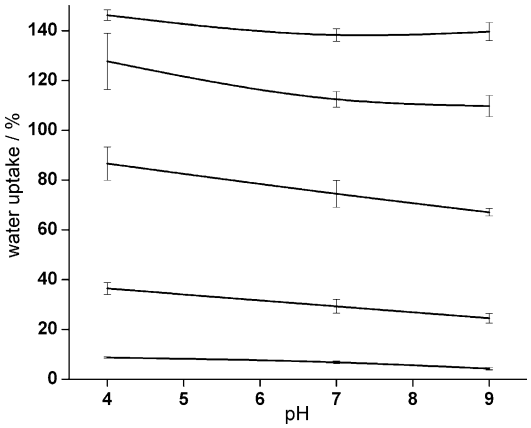

Figure 7. Water uptake of a) CS, b) PSf/TiO_2/CS, c) PSf/CS, d) PSf/TiO_2, and e) PSf membranes at various pH levels; error bars represent the SD.

basic pH it exists as CrO_4^{2-}, which shows an absorption peak at $\lambda_{max}=370$ nm (inset of Figure 8). In the acidic range it exists mainly in $HCrO_4^-$ and $Cr_2O_7^{2-}$ forms, which show two intense absorption peaks at $\lambda_{max}=255$ and 350 nm (Figure 8); these species have greater oxidation power[38] than CrO_4^{2-}, and hence chromium reduction is feasible only in acidic medium.

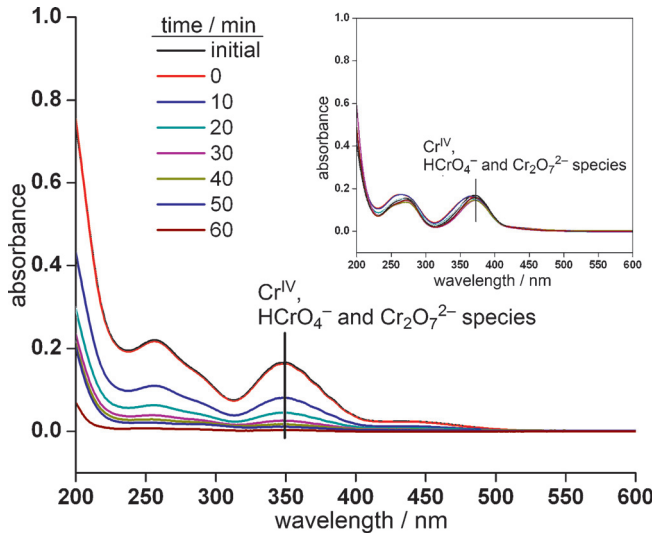

Figure 8. UV/Vis spectra for the reduction of Cr^{VI} carried out at acidic pH; inset: reduction of Cr^{VI} carried out at basic pH.

In this study the medium was maintained at pH 4 by the addition of formic acid to facilitate the formation of $HCrO_4^-$ and $Cr_2O_7^{2-}$ ions and reduction by the electron-donor groups present in the CS layer. As soon as the Cr^{VI} solution comes into contact with the CS layer, the reduction starts, which can be confirmed from Figure 8. The reduced Cr^{III} is present in Cr^{+3}, $Cr(OH)_2^{+}$, and $Cr(OH)^{+2}$ forms,[39] which are adsorbed onto the CS surface by complexation; this is supported by the change in membrane color from yellow to pale green, which is typical for Cr^{III} complexes.[40] The presence of Cr^{+3} can also be substantiated by the peak observed at $\lambda_{max}=580$ nm[41] in the UV/Vis spectra of the used membrane (Figure 9).

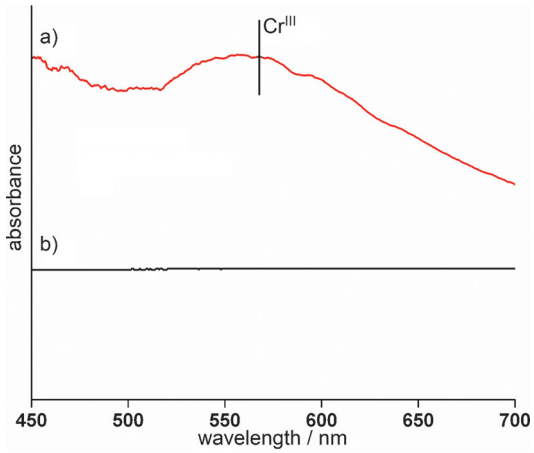

Figure 9. UV/Vis spectra for Cr^{III} adsorbed onto the membrane surface a) after and b) before Cr^{III} adsorption.

Figure 10 shows changes in the spectrum of the PSf/CS membrane after adsorption of Cr^{III} on the membrane surface. It is evident that peaks representing NH_2 and OH groups in CS underwent changes in their frequency and intensity. Most of

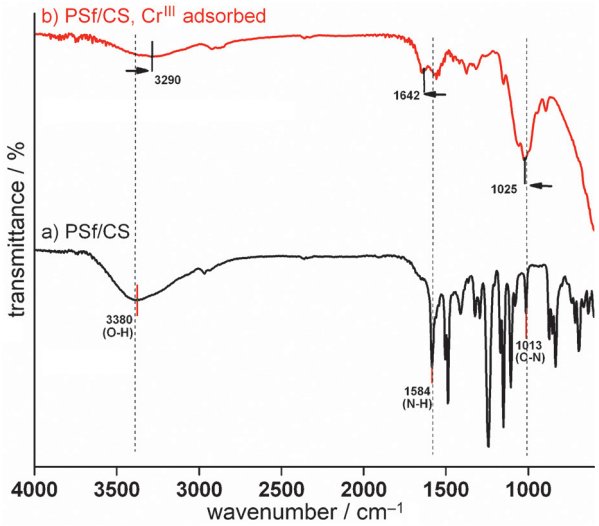

Figure 10. ATR-IR spectra of PSf/CS membranes a) before and b) after Cr^{III} adsorption.

the peaks show a decrease in intensity, and a shift in some has led to their merging into broad peaks. The peaks at 1013 cm^{-1} (C–N stretch) and 1584 cm^{-1} (N–H bending) show a shift in frequency toward higher values to 1025 and 1642 cm^{-1}, indicating that these peaks have taken part in the adsorption process. Furthermore, the broad region between 3000 and 3700 cm^{-1} representing the stretching frequencies of N–H and O–H groups shows changes toward a decrease in frequency. Thus, the adsorption of Cr^{III} ions was determined by the hydroxy and amine functional groups present in the CS layer.

The reduction process can be explained as follows: the NH_2 groups present in CS are protonated to NH_3^+ by formic acid to take part in the reduction of Cr^{VI} to Cr^{III}:

$$14\,NH_3^+ + 6\,e^- + Cr_2O_7^{2-} \rightarrow 2\,Cr^{3+} + 7\,H_2O \quad (2)$$

The free electrons are obtained from the OH groups present in the CS chain which act as electron-donor groups, and the NH_3^+ groups are converted back into NH_2 groups after reduction. These Cr^{III} species undergo complexation with the CS layer to impart the CS surface with its green color. Figure 8 clearly indicates that at basic pH the CrO_4^- species gets neither reduced nor adsorbed onto the CS surface, as there is no change in the concentration of Cr^{VI} solution. But under acidic conditions the existing $HCrO_4^-$ and $Cr_2O_7^{2-}$ species undergo reduction coupled with adsorption.

The error graph in Figure 11a represents the reduction of Cr^{VI} using PSf/TiO_2/CS membrane, and it is observed that in the presence of sunlight the reduced chromium undergoes back reaction and is recovered. This is due to the presence of TiO_2, which acts as a photocatalyst in the presence of sunlight. TiO_2 produces an e^-–h^+ pair upon excitation of light at $\lambda \geq 400$ nm. These electron hole pairs under aqueous conditions and atmospheric oxygen gives rise to a number of free radicals as follows:

$$TiO_2 \rightarrow TiO_2\,(h^+ + e^-) \quad (3)$$

$$H_2O + h^+ \rightarrow H^+ + OH^\bullet \quad (4)$$

$$OH^- + h^+ \rightarrow OH^\bullet \quad (5)$$

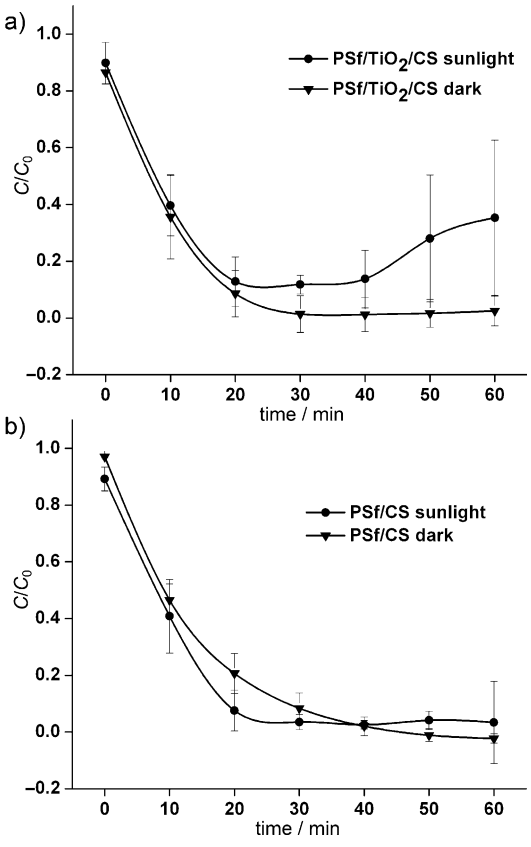

Figure 11. Reduction of Cr^{VI} in the dark and sunlight using a) PSf/TiO_2/CS and b) PSf/CS membranes; error bars represent the SD.

These free radicals are highly reactive and cause the back oxidation of Cr^{III} to Cr^{VI}, and this can happen only upon complete consumption of formic acid (confirmed by an increase in pH from 4 to 5.45 at the end of the reaction). At the beginning of the reaction, the presence of formic acid allows oxidant hole trapping to facilitate electron transfer to cause reduction.[42]

$$HCOOH \rightarrow HCOO^- + H^+ \quad (6)$$

$$HCOO^- + OH^\bullet \rightarrow H_2O + COO^\bullet \quad (7)$$

$$COO^\bullet \rightarrow \text{free } e^- + CO_2 \quad (8)$$

Thus no oxidation is observed at the beginning, but as formic is consumed, oxidation begins to occur to cause recovery of Cr^{VI}.

$$Cr^{III} + 3\,OH^\bullet \rightarrow Cr^{VI} + 3\,OH^- \quad (9)$$

However, the recovery of Cr^{VI} is only 20–30%. This is because the recovery process takes place simultaneously during adsorption, and the remaining Cr^{III} that is not adsorbed is recovered. Adsorbed Cr^{III} cannot be converted into Cr^{VI}. This substantiates the mechanism being followed is reduction followed by adsorption, because if adsorption of Cr^{VI} had to occur first followed by reduction to Cr^{III}, then the reduced Cr^{III} would not have been available to become oxidized back, which is observed in the case of sunlight-exposed reactions in the presence of TiO_2. Moreover, at acidic pH, the uptake of Cr^{VI} is difficult, as the amine groups are charged, thereby decreasing the number of complexation sites for $HCrO_4^-$ and $Cr_2O_7^{2-}$ ions. This was the case observed by Sivakami et al.,[43] with the adsorption of Cr^{VI} occurring at neutral pH, and to a slight extent at acidic pH over a long period of time. In the present case, however, there is continuous stirring on the membrane surface, and the short period of contact time does not favor Cr^{VI} adsorption. After the reduction process, as the amine groups lose their positive charge while formic acid is consumed, the adsorption of positively charged Cr^{III} ions is easier toward the electronegative nitrogen and oxygen atoms.

There is no recovery observed in the reduction process carried out in the dark, as TiO_2 is not active and does not play a role, as observed in Figure 11b. The reduction rate of Cr^{VI} to Cr^{III} remains the same. Hence PSf/CS membranes were used in the dark for further reactions, as recovery of chromium is not desired.

The prepared membranes were highly stable and were reused three times. After each reduction experiment the membranes were washed with distilled water, and the adsorbed Cr^{III} was recovered with a solution of H_2SO_4, dried for 24 h and used again. The membrane showed 100% reduction coupled with adsorption during recycling. Therefore, the recyclable efficiency of the membrane was good, but cracks were observed after three uses due to stirring, preventing further use. The prepared membranes show very good reliability toward complete removal of chromium, much better than the results reported by Sivakami et al.[43] using CS nanoparticles for Cr^{VI} ad-

sorption. Likewise, Zuo and Balasubramanian[44] reported the sorption of Cr^{III} using PCC beads. In both the cases, only Cr^{VI} adsorption was demonstrated, and the toxic Cr^{VI} remains unreduced. In contrast, the present study demonstrates an improved process for complete chromium removal by Cr^{VI} reduction to less toxic Cr^{III}, followed by adsorption. This process is also improved in terms of lower time consumption, better efficiency, and reusability.

Effect of competitive ions on Cr^{VI} reduction and adsorption

To investigate the scope of the prepared TFC membranes toward chromium removal, the studies were further extended to verify the effect of other competitive metal ions such as zinc and copper. The reduction was carried at regular time intervals as discussed in the Experimental Section below, and the results are shown in Figure 12. The reactions go to completion

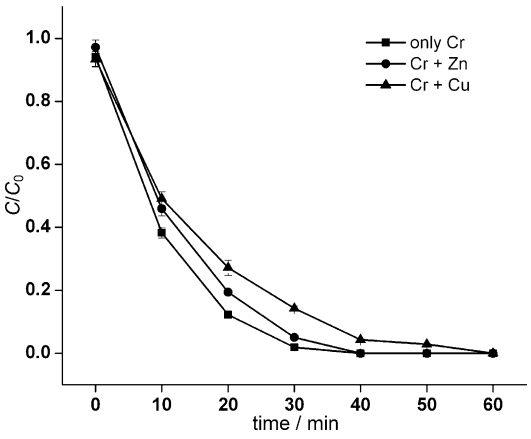

Figure 12. Reduction of Cr^{VI} using PSf/CS membrane in the presence of Cu^{II} and Zn^{II} metal ions at pH 4; error bars represent the SD.

in all cases. In the case of ion mixtures, however, it is evident that the amount of reduced Cr^{VI} to Cr^{III} at a particular time varies considerably in the case of both $K_2Cr_2O_7$–$ZnCl_2$ and $K_2Cr_2O_7$–$CuSO_4$ relative to a solution of $K_2Cr_2O_7$ alone. However, in the case of the $K_2Cr_2O_7$–$ZnCl_2$ mixture, the amount of time required for completion is 40 min, as is observed for the pure Cr^{VI} solution. Hence there is not much interference caused by Zn. On the other hand, in the case of the $K_2Cr_2O_7$–$CuSO_4$ mixture, the reaction continued for 60 min until completion. This may be attributed to hindrance caused by Cu^{II} ions, as they have high affinity for CS, as described by No and Meyers.[45] This hindrance may be due to the engagement of some of the active sites on the CS surface by the Cu^{II} ions, which decreases the rate of Cr^{VI} to Cr^{III} reduction. From the atomic absorption spectroscopy results it was confirmed that the maximum amount of adsorbed Cu^{II} and Zn^{II} was 61 and 43%, respectively, at the end of 60 min. Although the affinity of Cu^{II} ions for CS is very high, complete removal of Cu^{II} ions did not take place because maximum adsorption of Cu^{II} is favored at high pH, as observed by Ferrero et al.;[46] at higher pH, the concentration of H^+ ions is lower, increasing the availability of adsorption sites for Cu^{II} ions. As the pH is maintained at 4 in this case, however, most of the sites are occupied by H^+ ions, making it difficult for Cu^{II} ions to get adsorbed. It is also possible that the increased competition among the ions limits the reduction and simultaneous adsorption of specific ions requiring more time. From this result it is clear that affinity is not the sole criterion for adsorption, as pH plays a crucial role; the order of adsorption of ions in the above case is Cr > Cu > Zn at pH 4.

Kinetic study

The role of TiO_2 to cause both reduction and oxidation was further confirmed by kinetic studies. A straight line is obtained when $-\ln C/C_0$ is plotted vs. time for the reduction of Cr^{VI} to Cr^{III}, indicating that the reactions follow first-order kinetics (Figure 13 a,b). A positive slope was obtained from which the corresponding rate constants were determined for the reduction reactions, as listed in Table 2.

From Table 2 it can be seen that all the reactions have nearly same rate constants except for the reaction with TiO_2 NPs in the presence of sunlight. In this case, $OH^{\bullet}$ (oxidizing species) is produced, which simultaneously oxidizes Cr^{VI} to Cr^{III}, as discussed above, to decrease the reaction rate. Thus, the role of TiO_2 in enhancing the hydrophilicity and strength of the membranes is made most effective in suppressing its photoactivity by conducting the experiments in the dark.

Conclusions

The present study involved the design of novel, stable hydrophilic membranes for Cr^{VI} reduction and recovery of Cr^{III}. The prepared PSf/CS and PSf/TiO_2/CS membranes showed 100% chromium reduction at pH 4 in the absence of sunlight. The amine group present in the CS is responsible for reduction. Meanwhile, 100% adsorption of Cr^{III} on the membrane surface was observed, and this can be easily recovered. The presence of TiO_2 in the membrane was confirmed by XRD, and the incorporation of TiO_2 led to finger-like morphology as observed in SEM images of the membrane matrix. The thin-film composites were characterized for two separate layers of CS and PSf by SEM imaging. Contact angle studies revealed that the incorporation of TiO_2 NPs increased the hydrophilic nature of the membranes. The kinetics of the absorption showed a first-order rate constant. This study also paves the way for the use of the same toward rejection of chromium(VI), and this will be considered in the next set of studies by a dead-end filtration technique.

Experimental Section

Materials and methods

$TiCl_4$ (Loba Chemie) was used as titanium source for the preparation of TiO_2. CS and PSf were obtained from Sigma–Aldrich. The source for chromium(VI) is potassium dichromate, and reagents such as formic acid, acetic acid, and 1-methyl-2-pyrrolidone (NMP)

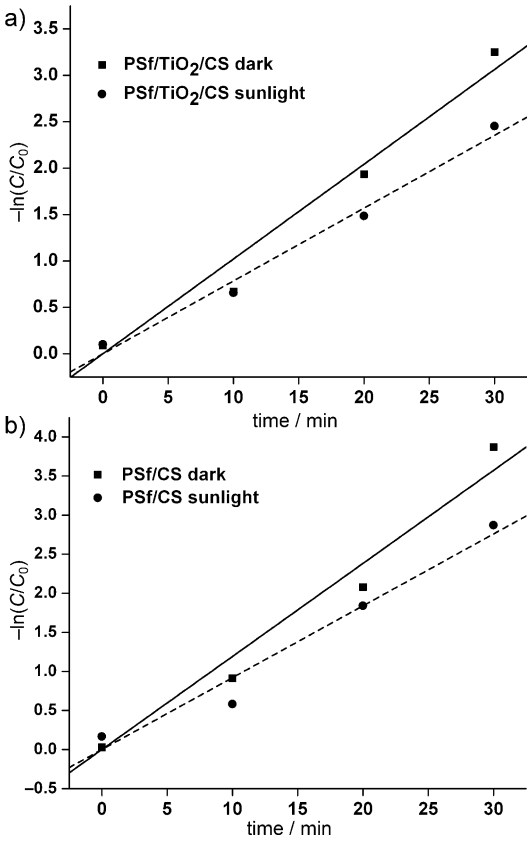

Figure 13. Plot of $-\ln C/C_0$ as a function of time over the course of Cr^{VI} reduction in the dark and under sunlight a) with or b) without TiO_2; linear regression was performed using OriginPro 8.

Table 2. Reaction order and rate constants (K) for the degradation of Cr^{VI} under various conditions.

Conditions	Light Source	Reaction Order	K [min^{-1}][a]
PSf/CS membrane + Cr^{VI} soln. + formic acid	sunlight	≈1.0	0.10
PSf/CS membrane + Cr^{VI} soln. + formic acid	dark	≈1.0	0.119
PSf/TiO_2/CS membrane + Cr^{VI} soln. + formic acid	sunlight	≈1.0	0.0784
PSf/TiO_2/CS membrane + Cr^{VI} soln. + formic acid	dark	≈1.0	0.102

[a] Rate constants obtained from plots of $-\ln C/C_0$ vs. irradiation time.

were purchased from Merck, and were used without further purification.

Preparation of TiO_2 NPs, PSf/TiO_2 and PSf membranes

Fine-grain powders of the anatase form of nano-TiO_2 were prepared by the gel-to-crystalline conversion method using $TiCl_4$, as described elsewhere.[47] In brief, $TiCl_4$ (100 mL) was added dropwise to 1 L of double-distilled water, and the temperature was maintained at $<10\,^{\circ}C$ throughout the hydrolysis. Concentrated H_2SO_4 was added to complete the hydrolysis followed by NH_4OH for precipitation until pH 7–8 was reached, as at this pH only TiO_2 will precipitate. The obtained precipitate was then filtered with Whatmann No. 41 filter paper (retention: 20–25 μm) and annealed at 600 °C for 6 h. The obtained powder was then ground and used for membrane preparation.

PSf/TiO_2 membranes were prepared by the phase-inversion method as discussed by Jyothi et al.[48] In brief, an optimum 500 mg of TiO_2 nanoparticles taken in 16 mL of NMP was stirred for 4 h at ambient temperature followed by sonication for 30 min to avoid agglomeration. PSf (4 g) was added to the sonicated solution, and stirred for 24 h at 60 °C to obtain a viscous solution. The obtained viscous solution was then casted on a glass plate using a glass rod. A further glass plate was dipped in a coagulation bath containing distilled water at room temperature. The membrane was peeled off by the phase-inversion method, and the obtained membrane was washed with distilled water and stored in distilled water for 24 h in order to gain mechanical strength. Similarly, PSf membranes were prepared by following the above procedure without the incorporation of TiO_2.

Preparation of CS thin-film composite membranes

CS (2 g) was dissolved in 100 mL of 1% acetic acid and stirred for 24 h at room temperature. The obtained solution was then filtered through G4 sand filter in order to remove the impurities and undissolved particles. The prepared PSf/TiO_2 membrane (100 cm^2) was pasted on the glass plate separately using tape with thickness of 1 mm. The stuck membrane was washed with distilled water and wiped with smooth tissue paper. A thin film of saturated PVA solution was brush coated on the substrate. CS (30 mL) was slowly poured in the center of the substrate and spread evenly throughout the substrate. Further, the TFC was dried at 60 °C for 4 h in a hot air oven. After drying, the membrane was allowed to reach room temperature, and was then washed with 1% NaOH to remove excess acetic acid. Finally the membrane was washed with distilled water until the washed water reached neutral pH. The same was repeated for bare PSf membranes. The obtained membranes were then subjected to characterization and performance studies (Table 3).

Membrane characterization

XRD and ATR-IR studies: X-ray diffraction (XRD) patterns of the membranes and TiO_2 NPs used in membrane preparation were recorded with a Shimadzu X-ray diffractometer, model XRD 7000, with CuKα radiation at a scan rate of $1^{\circ}\,min^{-1}$. The crystallite size of the TiO_2 particles was determined using Scherrer's equation.[49] ATR-IR spectra of the membranes was recorded using a Bruker ECO-ATR spectrophotometer in the range 600–4000 cm^{-1}. The membrane was dried in a vacuum desiccator for 48 h before recording the spectra.

Table 3. Composition of concentrations of the polymers and TiO_2 NPs in Membrane preparation.

Membrane	Composition			
	PSf [g]	TiO_2 NPs [mg]	NMP [mL]	CS Sol. [mL]
PSf	4	–	16	–
PSf/TiO_2	4	500	16	–
PSf/CS	4	–	16	30
PSf/TiO_2/CS	4	500	16	30

BET and SEM analysis: The surface area and pore volume of the TiO_2 NPs was analyzed using Smart Sorb 93 BET (Brunauer–Emmett–Teller) surface analyzer with sorb 93 reduction software. SEM images were recorded using a Shimadzu scanning electron microscope. The samples were first dipped and cracked in liquid nitrogen in order to get a clear image. The surfaces of the membranes were then gold sputtered and the images were captured.

Water uptake and contact angle: Water uptake properties were determined using distilled water at various pH values in order to obtain the hydrophilic properties of the membrane. Membranes were thoroughly washed with distilled water and then dried for 24 h in a vacuum desiccator. Dried membranes of area 1 cm^2 were cut and immersed in solutions of pH 4, 7, and 9 for 24 h. The swollen membranes were taken out; excess water was wiped off with tissue paper and membranes were weighed quickly. The degree of water uptake was calculated using the equation:

$$\% \text{ water uptake} = \left(\frac{W_w - W_d}{W_d}\right) \times 100 \quad (10)$$

in which W_w and W_d are the weights of wet and dried membranes, respectively.[50]

The contact angle of the membranes was recorded using an FTA-200 Dynamic contact angle goniometer according to the sessile droplet method. To minimize errors, contact angles were calculated at five different positions of the membrane, and average values are reported.

Removal of chromium

The removal of Cr^{VI} was carried out using PSf/TiO_2/CS and PSf/CS membranes. To evaluate the efficiency of the membranes in the dark and sunlight (intensity $> 700\ W\,m^{-2}$) the prepared membranes of 100 cm^2 area were cut and stuck to a trough using double-sided tape as represented in Figure 14. A Cr^{VI} solution (10 ppm) was used, and acidic and basic conditions were maintained with 0.1 N formic acid and NaOH solutions, respectively. After every 10 min, 10 mL of the sample were drawn and analyzed for the presence of chromium using UV/Vis spectroscopy (Shimadzu, Model UV-1800) at $\lambda_{max} = 350$ nm. C/C_0 was evaluated (where C = concentration of treated sample and C_0 = concentration of feed sample) and plotted against time to analyze the residual concentration of Cr^{VI}.[48]

To investigate the competitive adsorption behavior toward chromium removal, experiments were studied in presence of other metal ions such as copper and zinc. The complex mixture sets, namely $K_2Cr_2O_7$–$ZnCl_2$ and $K_2Cr_2O_7$–$CuSO_4$, were investigated, and an equal amount of chromium and other respective ions were used for analysis. Because the study was on the interference of different ions, pH (acidity), time (1 h), and concentration (10 ppm) were maintained constant as described. The concentration of metal ions was calculated using a 55 AA atomic absorption spectrophotometer (Agilent Technologies) in air–acetylene flame.

Desorption study: Desorption of Cr^{III} adsorbed on the CS layer was carried out by using a solution of 0.5 M H_2SO_4.[44] H_2SO_4 (100 mL, 0.5 M) was taken along with the TFC membrane stuck to the trough and stirred for 1 h. The concentration of desorbed of Cr^{III} was analyzed at specific time intervals by UV/Vis spectroscopy at $\lambda_{max} = 580$ nm.

Kinetic study: The rate constant K for the reduction process of Cr^{VI} was obtained as follows: The first-order rate law for the consumption of any reactant of concentration C is:

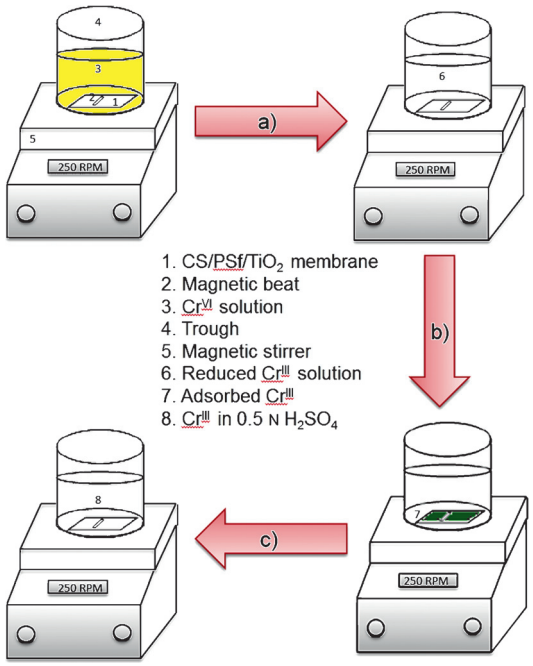

Figure 14. Experimental setup for the removal of Cr^{VI}: a) Cr^{VI} reduction to Cr^{III} in the dark; b) Cr^{III} adsorption onto the membrane surface; c) desorption of Cr^{III} from the membrane surface.

$$\frac{dC}{dt} = -KC \quad (11)$$

and upon integration it becomes:

$$\ln \frac{C}{C_0} = -Kt \quad (12)$$

from which $-\ln C/C_0$ vs. time t is plotted, and the kinetics can be discussed.[51]

Acknowledgements

The authors wish to acknowledge the Indian Ministry of Drinking water and Sanitation (no. 11017/33/2012-WQ) for financial support.

Keywords: chitosan · chromium · composite membranes · hydrophilicity · reduction

[1] K. Deshpande, S. Cheung, M. S. Rao, B. C. Dave, *J. Mater. Chem.* **2005**, *15*, 2997.
[2] F. Tan, X. Liu, X. Quan, J. Chen, X. Li, H. Zhao, *Anal. Methods* **2011**, *3*, 343.
[3] Z. Sun, L. Zheng, S. Zheng, R. L. Frost, *J. Colloid Interface Sci.* **2013**, *404*, 102.
[4] J. Bohdziewicz, *Desalination* **2000**, *129*, 227.
[5] L. Rafati, A. H. Mahvi, A. R. Asgari, S. S. Hosseini, *Int. J. Environ. Sci. Tech.* **2010**, *7*, 147.
[6] A. V. L. N. S. H. Hari Haran, D. Murali Krishna, *Int. J. Pharm Bio. Sci.* **2010**, *1*(2), S.No. 62.
[7] K. Dermentzis, A. A. Christoforidis, E. Valsamiddou, A. Lazaridou, N. Kokkinos, *Global Nest J.* **2011**, *13*, 412.
[8] M. Muthukrishnan, B. K. Guha, *Desalination* **2008**, *219*, 171.

[9] R. A. Shawabkeh, *J. Colloid Interface Sci.* **2006**, *299*, 530.
[10] H. A. Tsai, H. C. Chen, K. R. Lee, *Desalination* **2006**, *193*, 129.
[11] Y. Yang, P. Wang, *Polymer* **2006**, *47*, 2683.
[12] M. Padaki, A. M. Isloor, A. F. Ismail, M. S. Abdullah, *Desalination* **2012**, *295*, 35.
[13] J. Miao, G. Chen, C. Gao, S. Dong, *Desalination* **2008**, *233*, 147.
[14] S. S. Shenvi, S. A. Rashid, A. F. Ismail, M. A. Kassim, A. M. Isloor, *Desalination* **2013**, *315*, 135.
[15] P. Y. Zhuang, Y. L. Li, L. Fan, J. Lin, Q. L. Hu, *Int. J. Biol. Macromol.* **2012**, *50*, 658.
[16] M. Padaki, A. M. Isloor, P. Wanichapichart, *Desalination* **2011**, *279*, 409.
[17] M. Padaki, A. M. Isloor, J. Fernandes, K. N. Prabhu, *Desalination* **2011**, *280*, 419.
[18] F. Shi, Y. Ma, J. Ma, P. Wang, W. Sun, *J. Membr. Sci.* **2012**, *389*, 522.
[19] D. Yang, J. Li, Z. Jiang, L. X. Chen, *Chem. Eng. Sci.* **2009**, *64*, 3130.
[20] Y. H. Teow, A. L. Ahmad, J. K. Lim, B. S. Ooi, *Desalination* **2012**, *295*, 61.
[21] Z. Modrzejewska, W. Kaminski, *Ind. Eng. Chem. Res.* **1999**, *38*, 4946.
[22] S. Samadi, F. Khalilian, A. Tabatabaee, *J. Nanostruct. Chem.* **2014**, *4*, 84.
[23] A. M. Sajjan, M. Y. Kariduraganavar, *Development J. Membr. Sci.* **2013**, *438*, 8.
[24] B. H. Park, Y. J. Kim, J. S. Park, J. Choi, *J. Ind. Eng. Chem.* **2011**, *17*, 717.
[25] S. Jeck, P. Scharfer, W. Schabel, M. Kind, *Chem. Eng. Process.* **2011**, *50*, 543.
[26] L. P. Donald, G. M. Lampman, G. S. Kriz, J. R. Vyvyan, *Introduction to Spectroscopy*, Brooks/Cole Cengage Learning, Boston, **2008**.
[27] Y. Yang, H. Zhag, P. Wang, Q. Zheng, J. Li, *J. Membr. Sci.* **2007**, *288*, 231.
[28] V. D. Mote, Y. Purushotham, B. N. Dole, *J. Theor. Appl. Phys.* **2012**, *6*, 6.
[29] S. Rajesh, S. Senthilkumar, A. Jayalakshmi, M. T. Nirmala, A. F. Ismail, D. Mohan, *Colloids Surf. A* **2013**, *418*, 92.
[30] D. Emadzadeh, W. J. Lau, T. Matsuura, A. F. Ismail, M. R. Sisakht, *J. Membr. Sci.* **2014**, *449*, 74.
[31] V. Vatanpour, S. S. Madaeni, A. R. Khataee, E. Salehi, S. Zinadini, H. A. Monfared, *Desalination* **2012**, *292*, 19.
[32] H. Wu, J. Mansouri, V. Chen, *J. Membr. Sci.* **2013**, *433*, 135.
[33] M. Padaki, A. M. Isloor, K. K. Nagaraja, H. S. Nagaraja, M. Pattabi, *Desalination* **2011**, *274*, 177.
[34] X. Cao, J. Ma, X. Shi, Z. Ren, *Appl. Surf. Sci.* **2006**, *253*, 2003.
[35] R. Kumar, A. M. Isloor, A. F. Ismail, S. A. Rashid, A. A. Ahmed, *Desalination* **2013**, *316*, 76.
[36] M. Y. Arica, M. Yilmaz, E. Yalcin, G. Bayramoglu, *J. Membr. Sci.* **2004**, *240*, 169.
[37] D. Park, Y. S. Yun, H. W. Leeand, J. M. Park, *Bioresour. Technol.* **2008**, *99*, 1141.
[38] L. P. D'Souza, S. Shree, G. R. Balakrishna, *Ind. Eng. Chem. Res.* **2013**, *52*, 16162.
[39] Y. Hou, H. Liu, X. Zhao, J. Quand, J. P. Chen, *J. Colloid Interface Sci.* **2012**, *385*, 147.
[40] G. N. Kousalya, M. R. Gandhi, S. Meenakshi, *Int. J. Biol. Macromol.* **2010**, *47*, 308.
[41] S. T. Farrell, C. B. Breslin, *Environ. Sci. Technol.* **2004**, *38*, 4671.
[42] S. Rengaraj, S. Venkataraj, J. W. Yeon, Y. Kim, X. Z. Li, G. K. H. Pang, *Appl. Catal. B* **2007**, *77*, 157.
[43] M. S. Sivakami, T. Gomathi, J. Venkatesan, H. S. Jeong, S. K. Kim, P. N. Sudha, *Int. J. Biol. Macromol.* **2013**, *57*, 204.
[44] X. J. Zuo, R. Balasubramanian, *Carbohydr. Polym.* **2013**, *92*, 2181.
[45] H. K. No, S. P. Meyers, *Rev. Environ. Contam. Toxicol.* **2000**, *163*, 1–28.
[46] F. Ferrero, C. Tonetti, M. Periolatto, *Carbohydr. Polym.* **2014**, *110*, 367.
[47] R. Shwetharani, R. G. Balakrishna, *J. Photochem. Photobiol. A* **2014**, *295*, 11.
[48] M. S. Jyothi, M. Padaki, R. G. Balakrishna, R. K. Pai, *J. Mater. Res.* **2014**, *29*, 1537.
[49] N. Nakayama, T. Hayashi, *Colloids Surf. A* **2008**, *317*, 543.
[50] M. Padaki, A. M. Isloor, R. Kumar, A. F. Ismail, T. Matsuura, *J. Membr. Sci.* **2013**, *428*, 489.
[51] K. J. Laidler, *Chemical Kinetics*, Pearson Education and Dorling Kindersley, Delhi, **2009**.

Received: December 1, 2014
Published online on February 12, 2015

